

Pulsed nozzle Fourier transform microwave spectrometer: Ideal to define hydrogen bond radius

E. Arunan^{†,*}, A. P. Tiwari[†], P. K. Mandal[†] and P. C. Mathias[#]

[†]Department of Inorganic and Physical Chemistry and [#]Sophisticated Instruments Facility, Indian Institute of Science, Bangalore 560 012, India

A pulsed nozzle Fourier transform microwave (PNFTMW) spectrometer has been recently fabricated at the Indian Institute of Science. The basic design is the same as that of Balle and Flygare. However, recent advances in microwave and computer technologies have helped in designing a state-of-the-art PNFTMW spectrometer. The range of the spectrometer is from 2 to 26.5 GHz. Strong signals from OCS and several of its low abundant isotopes as well as weakly bound complexes such as Ar-(H₂O), Ar-H₂S and Ar₃-H₂S have been obtained. For the OCS parent isotopomer, the observed line width is only 2.8 kHz, indicating the high resolution of the spectrometer. Small hyperfine splittings could also be observed from the ¹³C spin-rotation interaction (4.9 kHz) in OCS and the *I* = 1 state of H₂O (10 kHz) in Ar-H₂O complex. This article gives the details of the newly fabricated PNFTMW spectrometer. By analysing the structural data available in the literature, most of it using PNFTMW spectrometer, we had recently defined a 'hydrogen bond radius' for all the hydrogen halides. This approach is extended to acetylene and water in this article, as models for the OH and CH groups involved in H bonding in biological systems. The H bond radius for H₂O is 0.78 ± 0.07 Å and that of C₂H₂ is 1.09 ± 0.05 Å.

MICROWAVE spectroscopy has traditionally been used to determine the structure of small molecules accurately^{1,2}. Only gaseous molecules or liquids and solids with finite vapour pressure could be studied. Hence, unlike spectrometers in other regions of the electromagnetic spectrum, microwave spectrometers did not become very popular. Commercial microwave spectrometers were available during the 60s and 70s and slowly they disappeared. Development of the pulsed nozzle Fourier transform microwave (PNFTMW) spectrometer by Balle and Flygare³, expanded the scope of microwave spectroscopy significantly. This spectrometer turned out to be almost ideal as it had very high sensitivity and resolution, simultaneously⁴. With this, one could look at weakly bound complexes (with non-zero permanent electric dipole

moment) formed between virtually any two chemicals, be they atoms, molecules, radicals or ions. Several laboratories around the world have built such spectrometers, mainly in the last decade or so⁵⁻¹⁴. This spectrometer is primarily a research equipment and hence is not commercially available. Recently, our laboratory has fabricated the PNFTMW spectrometer and this article describes the details.

The PNFTMW spectrometer has enabled accurate determination of the equilibrium structures of many different intermolecular complexes, bound by H bonding or van der Waals interaction. Locating the H atom in molecules and complexes is very difficult irrespective of the technique used, such as X-ray diffraction or rotational spectroscopy. However, with the sensitivity and resolution of PNFTMW spectrometer, small hyperfine interactions due to quadrupole coupling, spin-spin interactions, etc. could be well resolved. The hyperfine coupling constants observed in complexes provide independent structural data, which can refine/restrict the structure obtained from rotational constants¹². This has led to a wealth of accurate structural data for a large number of HX complexes. After a detailed analysis of these data, we have defined 'hydrogen bond radii' for the hydrogen halides (HF, HCl, HBr and HI)¹⁵. The B-HX distances (*r_H*) in these complexes could be interpreted as the sum of the 'hydrogen bond radius' of HX and the *r_{ESP}* of B, which is the distance from the bonding centre in B to the minimum in the electrostatic potential¹⁶. In this article, the analysis is extended to complexes containing H₂O and C₂H₂. Hydrogen bonds formed by OH and CH groups are prevalent in biological systems. The 'H bond radius' of H₂O and C₂H₂ could be used as an indicator of H bonds in biological systems.

Design and performance of the spectrometer

The PNFTMW spectrometer combines the supersonic expansion technique with the cavity Fourier transform microwave spectrometer. It has several components: (i) a Fabry-Perot cavity made of two highly polished aluminium mirrors (surface roughness better than microns), one of which is movable; (ii) supersonic nozzle source

*For correspondence. (e-mail: arunan@ipc.iisc.ernet.in)

for producing a cold jet/beam of molecules; (iii) high vacuum chamber pumped by a 20" diffusion pump housing both (i) and (ii); and (iv) microwave electrical circuit for polarizing the molecules and for detecting the molecular emission. The complete design of the spectrometer is described below in two parts – mechanical and electrical.

Mechanical design

The mechanical design of the vacuum chamber housing the Fabry–Perot cavity is shown in Figure 1. It is a cylindrical chamber made of stainless steel, SS 304. It is 1000 mm long and the diameter is 850 mm. The chamber is directly seated on top of the 20" diffusion pump (Vacuum Techniques, Bangalore). The pumping speed of the diffusion pump is $\approx 10,000 \text{ l s}^{-1}$ and it is backed by a 1000 l m^{-1} belt-less rotary mechanical pump. The chamber can be evacuated to 10^{-6} Torr and a liquid nitrogen trap improves the pumping below 10^{-5} Torr. The diffusion pump is water-cooled and a closed-circuit water circulation facility includes a cooling tower to keep the water at room temperature. Inside the chamber, two spher-

ical aluminium mirrors have been mounted co-axially on 3 SS guide rods. The mirrors are made from 65 mm thick aluminium disks with a diameter of 500 mm. The radius of curvature of both the mirrors is 800 mm and CNC machining ensured that the surface roughness and the radius were good to 1 micron. The distance between the mirrors could be varied in steps of microns between 650 and 750 mm. We have opted for a large mirror, so that the low frequency cut-off for the spectrometer is about 3.8 GHz. The radius of the mirror (a) and its radius of curvature (R) determine the lower frequency at which the Fresnel number is unity⁶:

$$a^2/R\lambda = 1. \quad (1)$$

Several laboratories have smaller mirrors with a low frequency cut-off near 8 GHz and the frequency range of such spectrometers is typically 6–18 GHz. The lower frequency limit is important, if one is interested in looking at larger clusters, which would have many low J transitions below 4 GHz. The Fabry–Perot cavity has been tested between 2 and 26 GHz in our spectrometer.

The movable mirror is fixed with a micrometer-controlled, fine-pitch screw rod and it is driven by a synchronized stepper motor (103H8221-5041, Sanyo

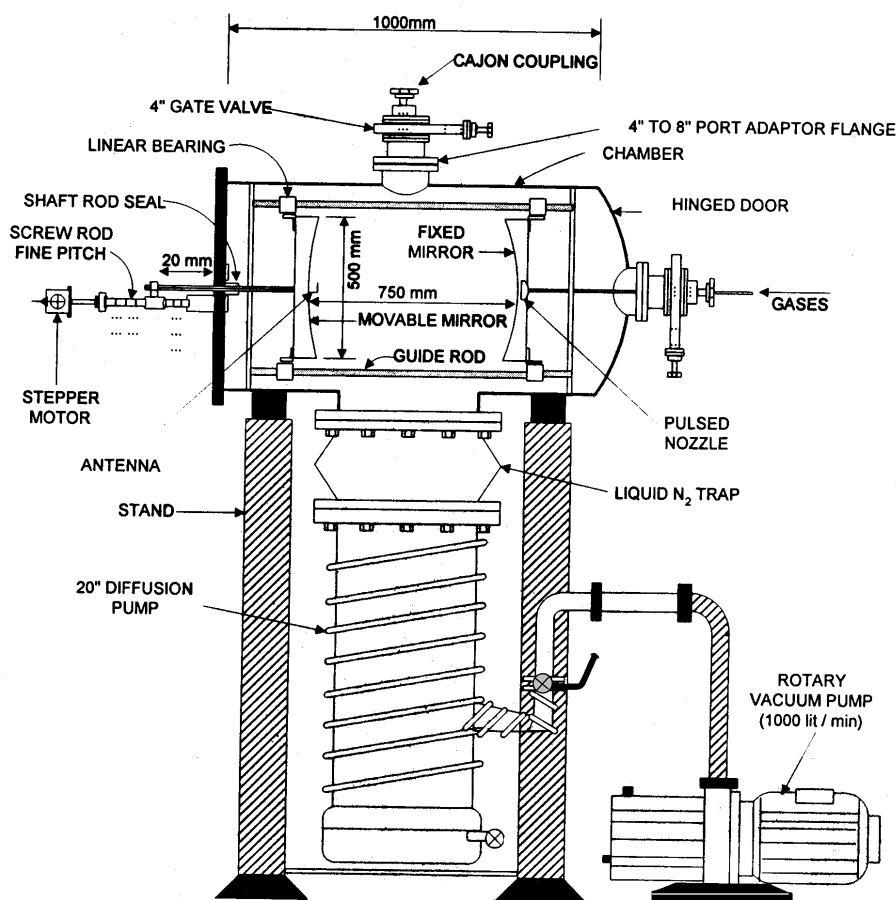


Figure 1. Schematic diagram of the mechanical design of PNFTMW spectrometer.

Denki, Japan). The stepper motor driver (PMM-BA-4803) is controlled by a PC. The linear screw rod has a pitch of 5 mm, which means that the linear distance covered by the mirror for a 360° rotation is 5 mm. The stepper motor, in high-resolution mode, takes 4000 steps for a complete rotation and thus the mirror moves in steps of 1.25 μm .

A coaxial cable runs through the supporting rod for the mirror with a SMA female connector at its end. This cable has a hermetically sealed SMA connector at the other end so that the microwave power can be coupled in and out of the cavity at vacuum. The SMA connector goes through a small hole at the centre of the mirror and an antenna (L-shaped bent wire made from the central wire of the coaxial cable) can be placed at the connector. The other mirror has a 10 mm hole at the centre as well. In addition, the backside of this mirror has a 25 mm cylinder carved out so that a pulsed nozzle (General Valve, USA, Series 9) could be placed. The pulsed valve goes through a 4" gate valve and an 'O' ring seal. This assembly could also be connected at the top of the chamber through another 4" gate valve.

A four-channel mass-flow controller/reader (MKS Instruments, 647B) and four different mass-flow meters (1179A) are used for preparing the gaseous mixture on the fly. Two of them are used for the carrier gases (either helium or argon) and their range is 0–1000 SCCM calibrated for N_2 . The other two are used for reagent gas(es) flow and they have a range of 0–20 SCCM. The output from all the four flow meters are mixed and taken to the pulsed valve. The reagent-flow meters are connected to 3-way valves in order to handle gases and liquids. The gaseous reagents are directly flown to the mixer and for liquids, the carrier gas is bubbled through a glass reser-

voir containing the liquid. The 3-way valves could be selected either for direct flow or through the liquid bubbler. The pulsed valve feed-through has a 3-way valve as well, so that the excess gases can be pumped out with a separate mechanical pump. This bleed line goes through a needle valve to control the outflow so that the back pressure at the nozzle could be maintained at the required level (typically 1–2 atm.).

Electrical design

The microwave/rf circuit used for polarization and detection of the molecules/complexes is shown in Figure 2. The microwave source is a frequency synthesizer (#1 in Figure 2, HP 83630L, 13 dBm power) which can generate any frequency between 10 MHz and 26.5 GHz to 1 Hz accuracy. The output from the synthesizer (at ν) is routed to a single pole double throw (SPDT) switch (#7, Sierra Microwave Technology, SFD0526-001, Isolation 60 dB), which powers either a single-side band generator (#5 Miteq, SM-0226-LC1A) or an image rejection mixer (#11 Miteq, IR-0226-LC1A). The SSBM mixes the synthesizer output at ν with a synchronous 30 MHz signal (Stanford Research Systems DS345) and generates $\nu + 30$ MHz signal. This signal is amplified by a medium power amplifier (#6, Miteq, JS3-02002600-5-7A) with a gain of 24 dB. The amplified signal goes through another SPDT switch (similar to #7). Both switches work synchronously connecting the polarization and detection parts (top and bottom of the SPDT switches in Figure 2), alternatively. During the polarization pulse, the SPDT output goes through a directional coupler (#8, Narda,

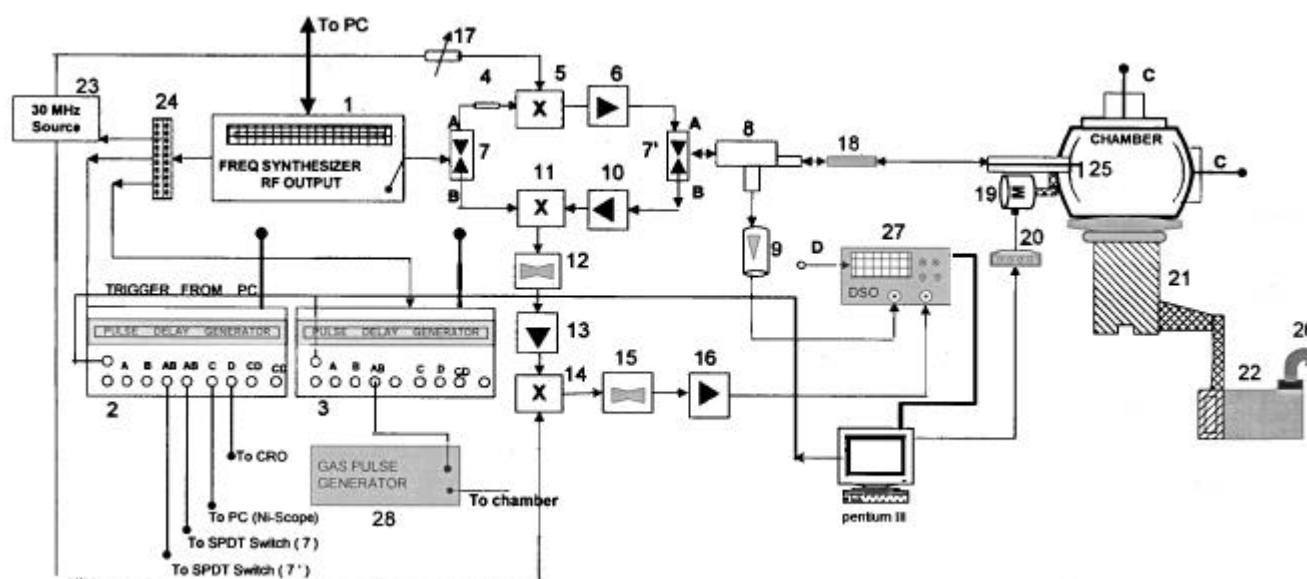


Figure 2. Schematic diagram of the microwave/rf circuit of the PNFTMW spectrometer (see text for description of the various components/instruments).

4227–16) and a DC block (#18, HP 11742 A) to the antenna inside the chamber.

The same antenna couples the molecular signal back to the detection circuit. During the polarization pulse, if the Fabry–Perot cavity is not tuned to the particular frequency $\nu + 30$ MHz, most of the mw power is reflected. The directional coupler routes 2.5% of this reflected signal to the oscilloscope (#27, Tektronix, TDS 430A) via a diode detector (#9, Narda, 4507). The movable mirror is moved in steps of micron until the reflected power shows a dip in the scope. The resonant frequencies, ν , of the Fabry–Perot resonator for the TEM_{mnp} modes are³:

$$\nu = c/2d [(q + 1) + (1/p)(m + n + 1) \cos^{-1}(d/R)]. \quad (2)$$

Here, d is the distance between the mirrors and R is the radius of curvature; m , n and q are the number of nodes in the three perpendicular axes. Thus, within the maximum variation of the distance between the mirrors (100 mm), several resonances can be observed for a given frequency. Most of the laboratories having a PNFTMW spectrometer^{5–14} employ 2 antennas, one in each mirror, for tuning and detection. This leads to an inherent reduction in the detected signal. Using the directional coupler with only one antenna is more advantageous. Only 2.5% of the signal is used for tuning purpose instead of almost half the signal.

The microwave pulse length of $\approx 1 \mu\text{s}$ leads to a frequency width of about 1 MHz and if there is an allowed transition within this bandwidth for the molecules/complexes in the cavity, polarization occurs. The polarized molecules emit a free induction decay (FID) at a frequency $\nu + 30 \pm \Delta$, which lasts for a few 100 μs . This signal is amplified by a low noise amplifier (#10, Miteq JS4-02002600-3-5P, noise 2.8 dB, gain 28 dB) and mixed with the synthesizer signal at ν in an image rejection mixer (#11, Miteq, IRO-0226-LC1A). The IRM gives only the $30 \pm \Delta$ signal which passes through a band pass filter (#12, Minicircuits, BBP 30) and a low noise amplifier (#13, Minicircuits, ZFL-500LN). The $30 \pm \Delta$ signal is down-converted to Δ by the rf mixer (#14, Minicircuits, ZAD-1) and a low pass filter (#15, Minicircuits, BLP-5). This signal is amplified and digitized by the oscilloscope. The 30 MHz signal is from the function generator (#23, SRS DS345) and so we have the option of varying the intermediate frequency (IF) in the mixer.

All the microwave components used in our set-up are ultra-wide band. The original spectrometer could be operated only in octave bandwidths and several switches were used for going from one band to another. In some cases, the components needed to be physically changed for going from one band to another. All the recently built PNFTMW spectrometers^{5,6} use one set of components that perform reasonably well throughout the frequency range. Our spectrometer can be operated from 2 to 26 GHz without changing any components.

This is an experiment of pulses with both the molecular sample and the microwave source being pulsed. Two delay generators (#2 and #3, SRS, DG535) generate all the timing sequences (shown in Figure 3) needed for the experiment. The sequence is described below with typical pulse lengths and delays. First a microwave pulse is applied to the evacuated chamber and the background response from the chamber is digitized. This includes random noise as well as coherent ringing from the cavity. The ringing typically lasts for a few microseconds. The digitizer is triggered after a delay to avoid the ringing. The pulsed nozzle is opened for 600 μs . After a delay of 1 ms for the molecules to reach the centre of the cavity, the microwave pulse is applied again. The response from the molecules is digitized now and the background collected earlier is subtracted. Fourier transformation of this time domain signal gives the frequency domain spectrum. The experiment can be repeated for N number of gas pulses to improve the signal-to-noise ratio. Moreover, the molecules stay in the cavity for 1–2 ms and it is possible to apply several microwave pulses per gas pulse.

The spectrometer operation is fully automated. Lab-Windows CVI (National Instruments) software offers the backbone using which the software has been developed. The code is written in C. The MW synthesizer, oscilloscope and the delay generators are controlled by a GPIB (NI) interface. The stepper motor driver is controlled by the parallel port, which also sends the starting trigger for the experiments. The time domain signal from the scope is transferred to the PC for averaging and Fourier transformation.

Performance of the spectrometer

The time domain signal obtained from the standard OCS is shown in Figure 4. The frequency domain spectrum shown in Figure 5 reveals the resolution of the spectrometer. The FWHM is only 2.8 kHz. The line centre could be determined to 0.1 kHz as is typical for the PNFTMW

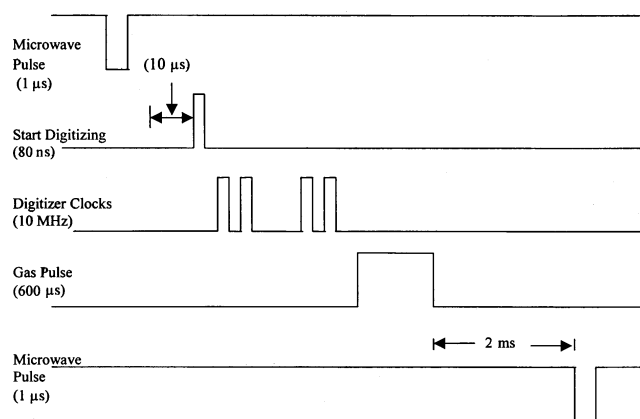


Figure 3. Pulse sequence of a typical experiment.

spectrometers. The doubling of the signal is due to Doppler effect, which is also typical of such spectrometers. The standing wave in the cavity is the super-position of two travelling waves going in opposite directions leading to Doppler doubling. This could be reduced with a skimmer if the pulsed valve is kept on top of the chamber. The real molecular frequency, 12162.9789 MHz, is the mean value of the two Doppler peaks. The signal from ^{18}OCS at 11409.7097 MHz is shown in Figure 6. The natural abundance of ^{18}O is only 0.2% and this signal can be seen by averaging just 10 shots. All the isotopomers of OCS have been observed. The $J = 0 \rightarrow 1$ transition for O^{13}CS is shown in Figure 7. The line is split by a mere 4.9 kHz, but it is well resolved. The splitting is due to the spin-rotation interaction which couples the ^{13}C nuclear spin with the rotation of the molecule.

Signals from several weakly bound complexes such as $(\text{Ar})_n\text{-H}_2\text{O}$, where $n = 1-3$ (refs 17-19) have also been observed. Several naturally occurring isotopomers of these complexes could be seen as well. The $J = 0 \rightarrow 1$

transitions of the para ($I = 0$) and ortho ($I = 1$) states of $\text{Ar-H}_2\text{O}$ complexes are shown in Figures 8 and 9. Note the well-resolved hyperfine interaction from the $I = 1$ state. In order to test the performance of the spectrometer over the frequency range, $\text{Ar-H}_2\text{S}$ (ref. 20) signals were observed from 3 to 20 GHz. Two different antennas were used to cover this frequency range⁶.

Hydrogen bond radii

Pauling, in his classic book²¹, has defined covalent, ionic and metallic radii for most of the atoms. These are quite useful in predicting the inter-atomic distances in molecules formed by covalent or ionic bonds. Unlike the bonding within the molecules, which is fairly well understood today, understanding intermolecular interaction is still an active area of research. The PNFTMW spectrometer has given reliable structural data on a number of weakly bound complexes, such as hydrogen bonded or

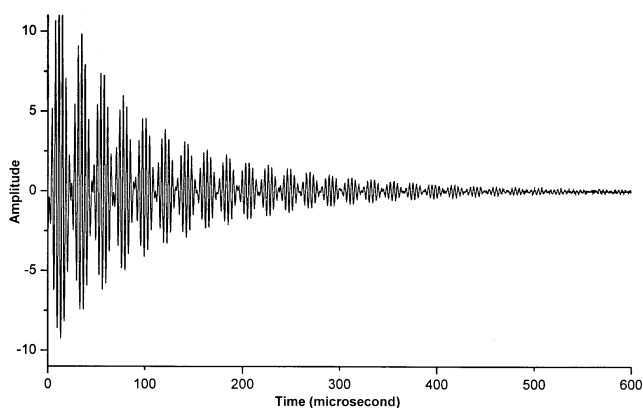


Figure 4. FID from the OCS polarized at 12162.7 MHz with a microwave pulse of 0.5 μs . Backing pressure was 1 atm. 3% OCS in Argon was used.

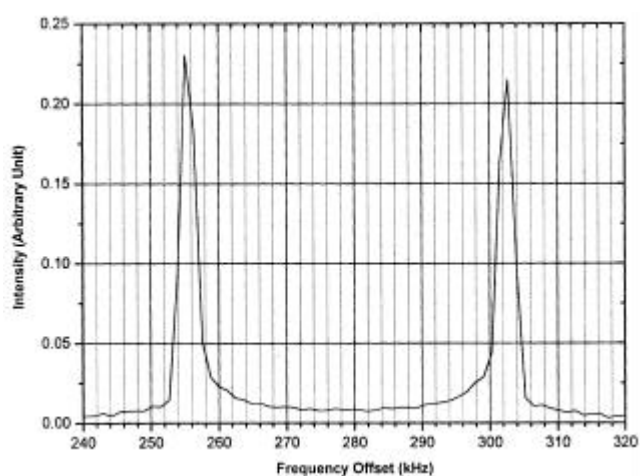


Figure 5. The frequency domain spectrum of Figure 4 showing the Doppler doublets of the $J = 0 \rightarrow 1$ transition of OCS at 12162.9789 MHz.

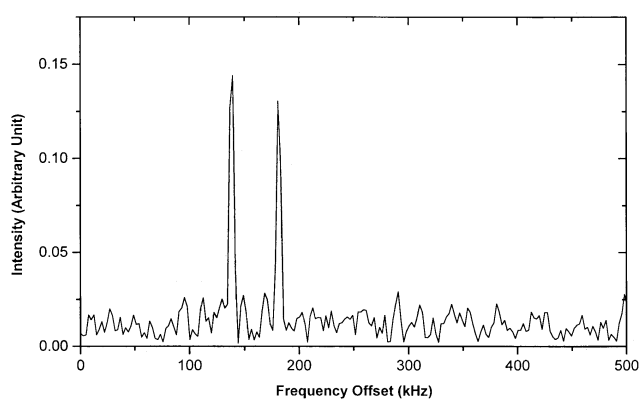


Figure 6. $J = 0 \rightarrow 1$ transition for the ^{18}OCS observed at 11409.7097 MHz with the natural sample of OCS. MO frequency was 11409.550 MHz

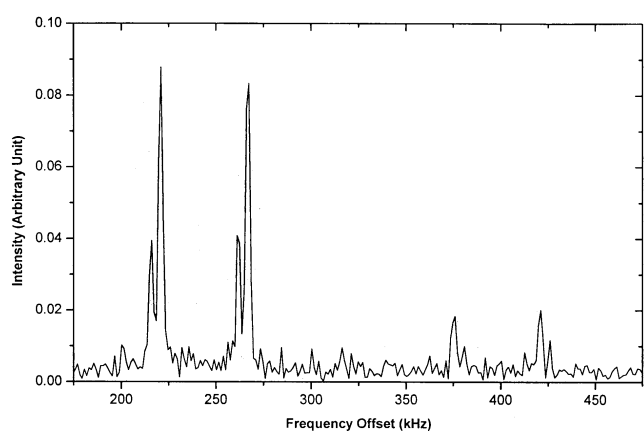


Figure 7. $J = 0 \rightarrow 1$ transitions for the O^{13}CS observed with the natural sample of OCS at 12132.8388 and 12132.8437 MHz. Doubling of the line is due to spin-rotation interaction from ^{13}C . MO frequency was 12123.6 MHz.

van der Waals. With these structural data, there have been several attempts to interpret the intermolecular distances. Buckingham and Fowler²² examined the X–F distances in several X–HF complexes and found that they were nearly the same as the sum of the van der Waals radii for X and F. The agreement was good to 0.1 Å. Legon²³ had used this analogy and extended this approach to all the hydrogen halides. For HCl and HBr, the difference between the sum of van der Waals radii and the X–Y distance was 0.2 Å or more.

Gadre and Bhadane¹⁶ interpreted the X–H distances in X–HF complexes differently. They calculated the molecular electrostatic potentials for the proton acceptor molecules B and defined r_{ESP} as the distance from the bonding

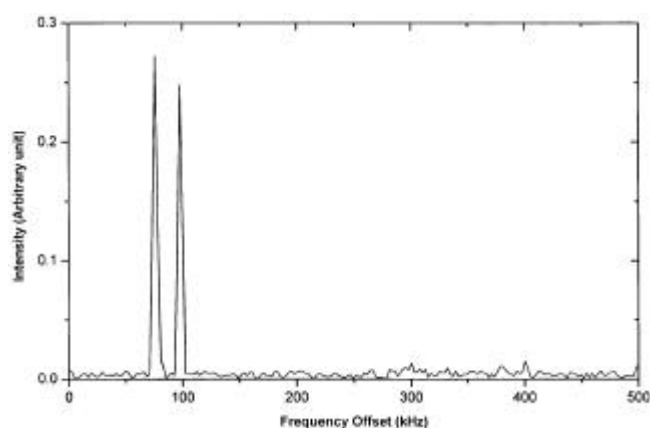


Figure 8. $J = 0 \rightarrow 1$ transition of the Ar–H₂O complex with H₂O in the lowest para 0_{00} state ($I = 0$) showing a sharp singlet at 5976.1866 MHz. MO frequency was 5976.1 MHz

centre (either an atom or a p bond centre) in B to the minimum in the electrostatic potential. When the bonding centre is an atom, the r_{ESP} was closer to the van der Waals radius of the atom. The B–H distance (r_{H}) was then interpreted as the sum of r_{ESP} for B and the van der Waals radius of H. A plot of r_{H} vs r_{ESP} was linear with a slope of 1.04 and an intercept of 0.47 Å. Thus, they concluded that the van der Waals radius of H, estimated in this manner, was 0.47 Å. This is much smaller than the preferred value of 1.2 Å (ref. 21) We felt that 0.47 Å could be assigned as the ‘hydrogen bond radius’ of HF. Hence, the analysis was extended to HCl, HBr and HCN complexes to estimate the ‘H bond radii’ for the three molecules as 0.74, 0.80 and 0.93 Å, respectively. Moreover, it was noted that the H bond radius had an empirical correlation with the dipole moment of the hydrogen halides¹⁵. From this correlation, the H bond radius for HI is estimated to be 0.90 ± 0.11 Å. This was in reasonable agreement with the limited data available for HI complexes.

Having estimated the H bond radii for all the hydrogen halides, here we extend the analysis to complexes having H bonds with OH and CH groups, for example H₂O and C₂H₂ as the donors. Table 1 lists the B–H distances (r_{H}) observed in several HX, H₂O and C₂H₂ complexes along with the r_{ESP} values for B taken from Gadre and Bhadane¹⁶. The HX data have been discussed earlier¹⁵. Figure 10 shows a plot of $(r_{\text{H}} - r_{\text{ESP}})$ vs r_{ESP} for H₂O and C₂H₂. The C₂H₂ data are displaced by 1.0 Å for clarity. The intercepts for H₂O and C₂H₂ are 0.78 ± 0.07 and 1.09 ± 0.05 Å. Naturally, the C–H bond with a nearly zero dipole moment leads to the H bond radius, which is nearly the same as that of the van der Waals radius of H.

Table 1. The r_{ESP} values of the bases (B) and the H-bond distances (r_{H}) for the H-bonded complexes B–HX. All the distances are in Å

B	r_{ESP}^a	r_{H} of B–HX						
		X = F	X = Cl	X = Br	X = I	X = CN	X = OH	X = C ₂ H
HF	1.27	1.86	2.08		0			
H ₂ O	1.27	1.74	1.93	1.99	2.13 (ref. 31)	2.08	2.02 (ref. 37)	
HCN	1.36	1.87	2.13	2.19	2.29 (ref. 32)	2.24		2.42 (ref. 47)
H ₃ N	1.25	1.78	1.85	1.83		2.16	2.03 (ref. 38)	2.33 (ref. 48)
OC	1.54	2.12	2.41	2.49	2.65 (ref. 33)	2.61	2.41 (ref. 39)	2.71 (ref. 49)
C ₂ H ₂	1.60	2.20	2.42			2.59		2.72 (ref. 50)
C ₂ H ₄	1.62	2.22	2.44	2.49		2.64	2.48 (ref. 40)	2.78 (ref. 51)
H ₂ S	1.79	2.32	2.53	2.57		2.75		
CH ₃ CN	1.34	1.83	2.01	2.07		2.21	2.07 (ref. 41)	2.37 (ref. 47)
C ₃ H ₆	1.52	2.10	2.28			2.41	2.34 (ref. 42)	
SO ₂	1.32	1.89	2.10					
C ₆ H ₆	1.93	2.65	2.71	2.72		2.79	2.65 (ref. 43)	
B ₂ H ₆	2.08	2.50	2.69					
CO ₂	1.46	1.91	2.15			2.35		
N ₂ O	1.40	1.94	2.08					
H ₂ CO	1.26	1.73	1.97				2.01 (ref. 44)	
N ₂	1.57	2.16	2.42	2.52		2.55	2.42 (ref. 45)	2.60 (ref. 52)
PH ₃	1.85	2.38 (ref. 24)	2.60 (ref. 27)	2.63 (ref. 27)	2.76 (ref. 34)	2.85 (ref. 34)		
(CH ₂) ₂ S	1.67	2.19 (ref. 25)	2.33 (ref. 28)			2.62 (ref. 35)		
(CH ₂) ₂ O	1.22	1.70 (ref. 26)	1.84 (ref. 29)	1.89 (ref. 30)		1.97 (ref. 36)	1.92 (ref. 46)	

^a r_{ESP} values are from ref. 16. For the last 3 entries, r_{ESP} was provided by Gadre (private commun).

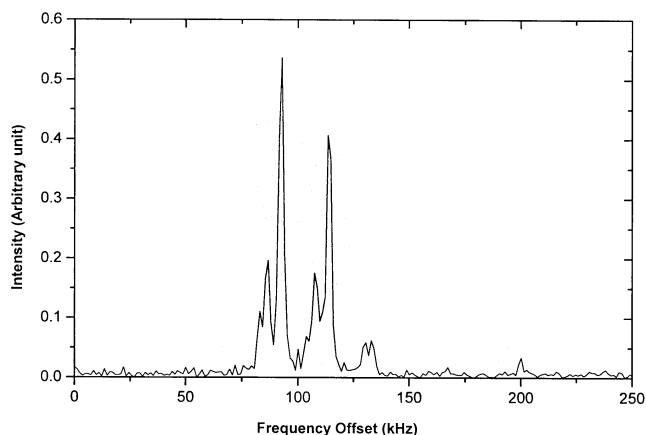


Figure 9. $J = 0 \rightarrow 1$ transition of Ar-H₂O complex with H₂O in the lowest ortho 1_{01} state ($I = 1$) showing a triplet at 5824.2430, 5824.2532 and 5824.2700 MHz. MO frequency was 5824.15 MHz.

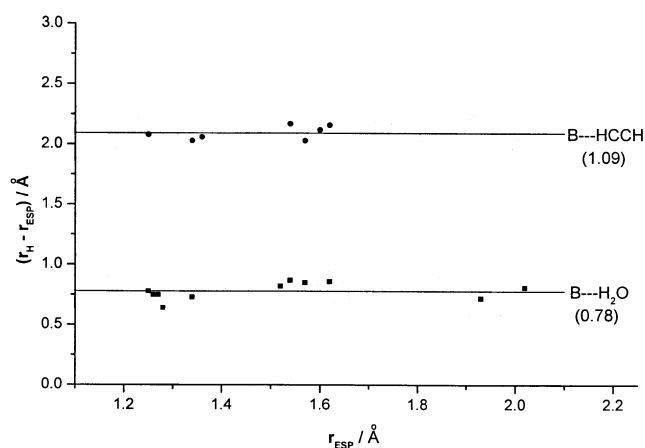


Figure 10. Plot of $(r_H - r_{ESP})$ vs r_{ESP} for several H₂O and C₂H₂ complexes. Intercept (given in parenthesis) is the 'H bond radius' for H₂O and C₂H₂. C₂H₂ is displaced by 1.0 Å in Y for clarity.

The dipole moment of H₂O is 1.85 D, which leads to a bond moment of 1.51 D for OH. Dipole moment correlation with the H bond radii would predict H₂O to have a much smaller H bond radius and H₂O does not fit in this correlation like HCN. Almost all the H₂O complexes exhibit tunnelling/internal rotation, which can interchange the protons. Such large amplitude motions could lead to an average distance, which is very different from the potential minimum. Such large amplitude motions are not possible in the biological systems (i.e. in condensed phase) and the effective H bond radius for OH could be shorter. The empirical correlation we have found could be useful for inference of an H bond with OH and CH groups.

Reliable structural data are available for a large number of HF and HCl complexes (Table 1). However, the data available for HBr, HI, H₂O and C₂H₂ complexes are limited. With the PNFTMW spectrometer, we hope to look at more H bonded and van der Waals complexes to

build up a large database which would be useful in improving fundamental understanding about intermolecular interactions.

Conclusions

The PNFTMW spectrometer has been recently fabricated in our laboratory. The range of the spectrometer is 2–26.5 GHz. Strong signals from the standard OCS and several weakly bound dimers (Ar–OCS), trimers (Ar₂–H₂O) and tetramers (Ar₃–H₂S) have been observed. The spectrometer has good sensitivity and resolution and rotational spectrum of any molecule or complex can be observed.

By analysing the accurate structural data available for a large number of complexes, we have defined H bond radii for all the hydrogen halides, HCN, H₂O and C₂H₂. This can be used to estimate the distance from the H of the donor to the bonding centre in the acceptor to better than 0.1 Å accuracy.

1. Townes, C. H. and Schawlow, A. L., *Microwave Spectroscopy*, McGraw Hill, New York, 1955.
2. Gordy, W. and Cook, R. L., *Microwave Molecular Spectra*, Wiley, New York, 1984.
3. Balle, T. J. and Flygare, W. H., *Rev. Sci. Instrum.*, 1981, **52**, 33–45.
4. Muentner, J. S. in *Structure and Dynamics of Weakly Bound Complexes* (ed. Weber, A.), Reidel, Dordrecht, 1987, pp. 3–21.
5. Suenram, R. D., Grabow, J-U., Zuban, A. and Leonov, I., *Rev. Sci. Instrum.*, 1999, **70**, 2127–2135.
6. Grabow, J-U., Stahl, W. and Dreizler, H., *ibid*, 1996, **67**, 4072–4084.
7. Alonso, J. L., Lorenzo, F. J., Lopez, J. C., Lesarri, A., Mata, S. and Dreizler, H., *Chem. Phys.*, 1997, **218**, 267–275.
8. Warner, H. E., Wang, Y., Ward, C., Gillies, C. W. and Interrante, L., *J. Phys. Chem.*, 1994, **98**, 12215–12222.
9. Hight Walker, A. R., Chen, W., Novick, S. E., Bean, B. D. and Marshall, M. D., *J. Chem. Phys.*, 1995, **102**, 7298–7305.
10. Harmony, M. D., Beran, K. A., Angst, D. M. and Ratzlaff, L., *Rev. Sci. Instrum.*, 1995, **66**, 5196–5202.
11. Lida, M., Ohshima, Y. and Endo, Y., *J. Chem. Phys.*, 1991, **94**, 6989–6944.
12. Legon, A. C., in *Atomic and Molecular Beam Methods* (ed. Scoles, G.), Oxford University Press, New York, 1992, vol. 2, pp. 289–308.
13. Bumgarner, R. E. and Kukolich, S. G., *J. Chem. Phys.*, 1987, **86**, 1083–1089.
14. Hillig, K. W., Matos, J., Scioly, A. and Kuczkowski, R. L., *Chem. Phys. Lett.*, 1987, **133**, 359–362.
15. Mandal, P. K. and Arunan, E., *J. Chem. Phys.*, 2001, **114**, 3880–3882.
16. Gadre, S. R. and Bhadane, P. K., *ibid*, 1997, **107**, 5625–5626.
17. Germann, T. C. and Gutowsky, H. S., *ibid*, 1993, **98**, 5235–5238.
18. Arunan, E., Dykstra, C. E., Emilsson, T. and Gutowsky, H. S., *ibid*, 1996, **105**, 8495–8501.
19. Arunan, E., Emilsson, T., Gutowsky, H. S. and Dykstra, C. E., *ibid*, 2001, **114**, 1242–1248.
20. Gutowsky, H. S., Emilsson, T. E. and Arunan, E., *ibid*, 1997, **106**, 5309–5315.
21. Pauling, L., in *The Nature of the Chemical Bond*, Cornell University Press, Ithaca, 1960, pp. 221–267.

22. Buckingham, A. D. and Fowler, P. W., *Can. J. Chem.*, 1985, **63**, 2018–2025.
23. Legon, A. C., *Angew. Chem., Int. Ed. Engl.*, 1999, **38**, 2686–2714.
24. Legon, A. C. and Willoughby, L. C., *Chem. Phys.*, 1983, **74**, 127–136.
25. Atkins, M. J., Legon, A. C. and Warner, H. E., *Chem. Phys. Lett.*, 1994, **229**, 267–272.
26. Legon, A. C. and Wallwork, A. L., *ibid*, 1991, **178**, 279–284.
27. Legon, A. C. and Willoughby, L. C., *J. Chem. Soc., Chem. Commun.*, 1982, 997–998.
28. Evans, C. M. and Legon, A. C., *Chem. Phys.*, 1995, **198**, 119–131.
29. Legon, A. C., Rego, C. A. and Wallwork, A. L., *J. Chem. Phys.*, 1992, **97**, 3050–3059.
30. Legon, A. C. and Wallwork, A. L., *J. Chem. Soc., Faraday Trans.*, 1990, **86**, 3975–3982.
31. McIntosh, A., Lucchese, R. R., Bevan, J. W., Suenram, R. D. and Legon, A. C., *Chem. Phys. Lett.*, 1999, **314**, 57–64.
32. Fowler, P. W., Legon, A. C. and Peebles, S. A., *ibid*, 1994, **226**, 501–508.
33. Wang, Z., Lucchese, R. R., Bevan, J. W., Suckley, A. P., Rego, C. A. and Legon, A. C., *J. Chem. Phys.*, 1993, **98**, 1761–1767.
34. Legon, A. C. and Willoughby, L. C., *Chem. Phys.*, 1984, **85**, 443–450.
35. Cosleou, J., Lister, D. J. and Legon, A. C., *Chem. Phys. Lett.*, 1994, **231**, 151–158.
36. Goodwin, E. J., Legon, A. C. and Millen, D. J., *J. Chem. Phys.*, 1986, **85**, 676–682.
37. Dyke, T. R. and Muentzer, J. S., *ibid*, 1974, **60**, 2929–2930.
38. Herbine, P. and Dyke, T. R., *ibid*, 1985, **83**, 3768–3774.
39. Yaron, D., Peterson, K. I., Zolanz, D., Klemperer, W., Lovas, F. J. and Suenram, R. D., *ibid*, 1990, **92**, 7095–7109.
40. Peterson, K. I. and Klemperer, W., *ibid*, 1986, **85**, 725–732.
41. Lovas, F. J. and Sobhanadri, J., *Proc. Ohio State Spectroscopy Symposium*, 1994, TC 12.
42. Andrews, A. M., Hilling II, K. W. and Kuczowski, R. L., *J. Am. Chem. Soc.*, 1992, **114**, 6765–6770.
43. Gutowsky, H. S., Emilsson, T. and Arunan, E., *J. Chem. Phys.*, 1993, **99**, 4883–4893.
44. Lovas, F. J. and Lugez, C. L., *J. Mol. Spectrosc.*, 1996, **179**, 320–323.
45. Leung, H. O., Marshall, M. D., Suenram, R. D. and Lovas, F. J., *J. Chem. Phys.*, 1989, **90**, 700–712.
46. Caminati, W., Moreschini, P., Rossi, I. and Favero, P. G., *J. Am. Chem. Soc.*, 1998, **120**, 11144–11148.
47. Howard, N. W. and Legon, A. C., *J. Chem. Phys.*, 1986, **85**, 6898–6904.
48. Fraser, G. T., Leopold, K. R. and Klemperer, W., *ibid*, 1984, **80**, 1423–1426.
49. Rochrig, M. A. and Kukolich, S. G., *Chem. Phys. Lett.*, 1992, **188**, 232–236.
50. Prichard, D. J., Nandi, R. N. and Muentzer, J. S., *J. Chem. Phys.*, 1988, **89**, 115–123.
51. Fraser, G. T., Lovas, F. J., Suenram, R. D., Gillies, J. Z. and Gillies, C. W., *Chem. Phys.*, 1992, **163**, 91–101.
52. Legon, A. C., Wallwork, A. L. and Fowler, P. W., *Chem. Phys. Lett.*, 1991, **184**, 175–181.

ACKNOWLEDGEMENTS. We thank the Department of Science and Technology for a generous grant and the Director, Indian Institute of Science for partial support. E. A. thanks Dr T. Emilsson for information regarding the PNFTMW spectrometer. Mr B. J. Mukkada, Mr Premendra Kumar, Mr Dharmendar J. Ramdass, Mr Utpal Sharma, Mr Saket Kumar and Ms S. Sivasankari have all helped at various stages of fabrication. E.A. thanks Dr R. D. Suenram, Prof. S. E. Novick, and Prof. W. Stahl for helpful discussions. We thank Prof. S. R. Gadre for sharing data on the electrostatic potential of PH_3 , $(\text{CH}_2)_2\text{O}$ and $(\text{CH}_2)_2\text{S}$.

Received 16 October 2001; accepted 1 February 2002